Hydrodynamic Relaxation of an Electron Plasma to a Near-Maximum Entropy State

D. J. Rodgers,[1] S. Servidio,[1] W. H. Matthaeus,[1] D. C. Montgomery,[2] T. B. Mitchell,[1,*] and T. Aziz[1]

[1]*Department of Physics and Astronomy, University of Delaware, Newark, Delaware 19716, USA*

[2]*Department of Physics and Astronomy, Dartmouth College, Hanover, New Hampshire 03755, USA*

(Received 13 March 2009; published 18 June 2009)

Dynamical relaxation of a pure electron plasma in a Malmberg-Penning trap is studied, comparing experiments, numerical simulations and statistical theories of weakly dissipative two-dimensional (2D) turbulence. Simulations confirm that the dynamics are approximated well by a 2D hydrodynamic model. Statistical analysis favors a theoretical picture of relaxation to a near-maximum entropy state with constrained energy, circulation, and angular momentum. This provides evidence that 2D electron fluid relaxation in a turbulent regime is governed by principles of maximum entropy.

DOI: 10.1103/PhysRevLett.102.244501 PACS numbers: 47.27.eb, 52.27.Jt, 52.35.Ra

Electron traps [1–3] allow for the experimental study of two-dimensional (2D) turbulence, when the leading order description of the plasma is that of a guiding center fluid. Then, the governing dynamical equations correspond to 2D hydrodynamics, up to constants of proportionality [1,4,5]. This is perhaps the simplest case of self-organizing turbulence, and is therefore a paradigm for Taylor relaxation [6], selective decay [7] and other fluid and plasma relaxation processes [8], with diverse implications ranging from superfluids [8], to astrophysics [9] and planetary atmospheres [10]. Two-dimensional relaxation has a well demonstrated sensitivity to the initial data [11] and electron trap dynamics are no exception. Special preparation can lead to quasistable states characterized by isolated vortices (or ''crystals'') [12–14], off axis states [15], or wavelike behavior [3]. However, here we are concerned with a broad class of meta-equilibria attained in cases in which nonlinear effects and turbulence are strong, and the system is initially not too close to one of the above mentioned special cases. We study the dynamics of these turbulent states (see also [16,17]) in a Malmberg-Penning electron trap (MPT) experimentally, analytically, and numerically. We seek evidence that the intermediate time relaxation to a long lived quasiequilibrium proceeds towards a state well described by a statistical mechanics principle of maximum entropy (for the periodic case, see [18–20]). The evidence supports the importance of including as a constraint the angular momentum, as well as the energy and total circulation.

Experimental data are from the University of Delaware electron trap [3]. Electrons are injected into a cylindrical (r, θ, z) vacuum chamber by a heated filament at one end of the device. Confinement in radius is enforced by a magnetic field $\boldsymbol{B}_0 = B\hat{z}$, and at the ends by electrodes with an applied voltage V_c. This maintains an approximately 2D state with the axial z coordinate ignorable. Following evolution of the electron distribution, measurements are made by electrostatically dumping the electrons onto the phosphor screen. The emitted light is proportional to the charge density, and is read by a CCD camera [3]. This differs from some experimental setups in which each cycle provides one or a few pixels of the distribution, and a single global picture requires many cycles (e.g., [1,2]). Here, for time sequences, additional cycles employ identical initial conditions and the (destructive) imaging diagnostic is enacted at successively later times.

The focus here is on, first, establishing that the dynamics of the electron distribution in the experiment is reasonably well described by 2D Navier-Stokes (NS) dynamics, with free-slip boundary conditions. To a reasonable degree of approximation, the electron density $n(r, \theta, t)$ follows 2D, z-averaged, $\boldsymbol{E} \times \boldsymbol{B}$ drift motion [1], where

$$\boldsymbol{v}_D = -\frac{c\boldsymbol{\nabla}\phi \times \hat{z}}{B}, \qquad \boldsymbol{\nabla}^2\phi = -4\pi qn, \tag{1}$$

where ϕ is the electrostatic potential, q is the charge of the electron, and $\boldsymbol{E} = -\boldsymbol{\nabla}\phi$. For this system, $\boldsymbol{v}_D$ is equivalent to the 2D fluid velocity $\boldsymbol{v}$, with the vorticity ω proportional to electron number density n, and stream function ψ proportional to $-\phi$ the potential. (Note the sign difference [1].) Because of this analogy, the evolution of the system will be assumed to be governed by the 2D NS equation for one-sign vorticity,

$$\frac{\partial\omega}{\partial t} + (\boldsymbol{v}\cdot\boldsymbol{\nabla})\omega = \nu\boldsymbol{\nabla}^2\omega, \tag{2}$$

where $\boldsymbol{v} = \boldsymbol{\nabla}\psi \times \hat{z}$ and $\boldsymbol{\nabla}^2\psi = -\omega$. The term involving viscosity ν is familiar in hydrodynamics but not well motivated in the guiding center plasma case, as the dissipation mechanisms may differ significantly in NS and MPT analyses [21]. Establishing this correspondence is a first step towards understanding the dynamical framework in which the observed relaxation processes might be understood. When $\nu = 0$ the system reduces to the ideal 2D Euler equations. In all cases we must impose $\psi = \text{const}$ on the impenetrable device boundary at $r = R$. This implies, in the electrodynamic analogy, that the (metal) boundary is an equipotential surface. If we impose no further condition, we have, for NS, a boundary that is free-slip, with unconstrained tangential velocity at the wall, and, for MPT, a

surface charge distribution that is proportional to the normal component of electric field.

For an ideal system with free-slip boundary conditions the averaged energy $E = \frac{1}{2}\langle\omega\psi\rangle$, circulation $C = \langle\omega\rangle$, and angular momentum $L = \langle\omega r^2\rangle$ are conserved through the evolution ($\langle\ldots\rangle = \frac{1}{\pi R^2}\int_0^R\int_0^{2\pi}\ldots rdrd\theta$). In the dissipative case, C, E, and L are slowly varying relative to entropy $S = -\langle\omega\ln\omega\rangle$ and enstrophy $\Omega = \frac{1}{2}\langle\omega^2\rangle$. All of the above quantities decay with time except S, which grows. Over longer time scales, E and C decrease, and eventually the system evolves towards a rigid rotator thermal equilibrium [1,22]. Here we are interested in relaxation at intermediate hydrodynamical time scales that is governed by approximate conservation laws.

If the electron experiment behaves like periodic 2D hydrodynamics [4,5,23,24], one would expect that C, E, and L will be approximately constant for time scales of interest, while S increases and Ω decreases. Indeed we typically see this ordering of time variations in the experimental electron data sets. An example is shown in Fig. 1, for the experiment labeled BZ (see Table I).

The central issue is to describe the physics that guides this relaxation in a turbulent system, and the question is whether the system goes toward a maximum entropy or a minimum enstrophy state. If the evolution minimizes the enstrophy [7], subject to the constraint that C, E, and L are constants [25], then the final state satisfies the differential equation

$$\omega = \delta + \xi\psi + \eta r^2, \tag{3}$$

where δ, ξ, and η are parameters determined by the constrained values of C, E, and L, employing the method of Lagrange multipliers. Axisymmetric solutions are given by linear combinations of Bessel functions, and typically these have negative values of ω near the boundary. A method for adjusting these solutions to maintain single-signed vorticity [2] has been criticized [16]. In fact, since the enstrophy is not proportional to the NS dissipation with free-slip (or stress free) boundaries—the rigidly rotating state has $\Omega \neq 0$ but zero dissipation—one might even question the dynamical basis for postulating a minimum enstrophy theory.

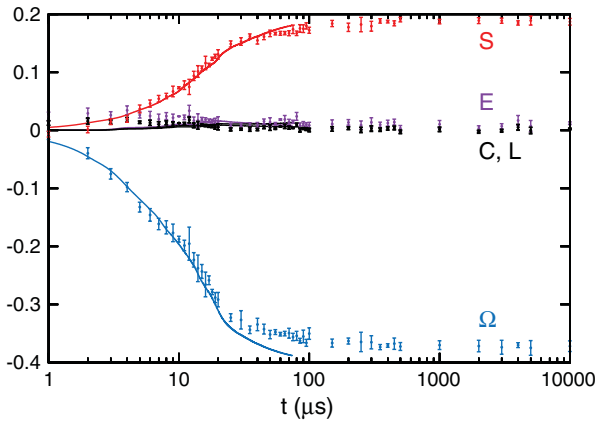

FIG. 1 (color). Relative variation $\frac{A(t)-A(0)}{A(0)}$ vs time, for global quantities A: E (violet), C and L (black), S (red) and Ω (blue). Symbols with error bars are experiment BZ (see Table I); solid lines are simulation data. C, E, and L are conserved within 5%, but variations in S and Ω are much larger.

Another possibility for describing the observed relaxation is based on a statistical argument [2,16]. Here, the system evolves towards a state of constrained maximum entropy [4,5,18,20]. This state satisfies the nonlinear differential equation for the parameters α, β, and γ:

$$\omega = e^{\alpha+\beta\psi+\gamma r^2}, \tag{4}$$

where again $\omega = -\nabla^2\psi$. General analytical solutions of Eq. (4), for single-signed vorticity in a bounded circular domain, have yet to be found. However the axisymmetric case, not restricting L (setting $\gamma = 0$) in Eq. (4), is a special solution to the *Liouville equation* [26], namely:

$$\omega(r) = \frac{\omega_0}{(1+\kappa^2 r^2)^2}. \tag{5}$$

Here ω_0 and κ are coefficients determined by C and E. This solution may approximate the most probable state if angular momentum is not constrained.

To inquire whether 2D NS dynamics, with a single-sign vorticity, can describe the evolution of the electron trap data, we carried out direct numerical simulation of incompressible 2D NS flow. The algorithm uses second order spatial finite difference in a polar domain, and second order Runge-Kutta in time (see Ref. [27]). We employ a stream function-vorticity representation, and free-slip boundary conditions ($\psi = 0$ at $r = R$) with a specified uniform dimensionless viscosity ($\nu \simeq 5\times10^{-4}$), with $N_r \times N_\theta = 512^2$ mesh points. This is a nonstandard procedure in hydrodynamics [28], as usually $\nu \neq 0$ would imply no-slip or stress free boundaries. However, no-slip conditions cannot be used here because they would immediately lead to production of positive and negative vorticity; the experiment, of course, contains only negative charges (electrons) in the interior, with opposite-signed neutralizing charges within the conducting walls (images charges). The chosen

TABLE I. Energy E, angular momentum L, initial and final enstrophy Ω and entropy S, and normalized fit errors χ^2_Ω & χ^2_S, for several experimental runs. Except for lowest E/L cases (e.g., Run D, a smooth hollowed vortex case, as in [2]), evolution tends more towards maximum S than minimum Ω. These higher E/L and Ω/E cases are more turbulent.

expt. label	E Init	L Init	Ω Init	Fin	$-S$ Init	Fin	χ^2_Ω Fin	χ^2_S Fin
BZ	0.30	0.08	5.28	3.34	1.98	1.61	0.63	0.29
CC	0.27	0.10	3.31	2.50	1.67	1.38	0.15	0.04
CE	0.24	0.13	2.93	2.30	1.47	1.12	0.91	0.37
CP	0.23	0.15	3.58	2.33	1.47	0.99	1.07	0.44
D	0.22	0.14	1.72	1.54	1.12	1.02	0.08	0.07

viscosity is as small as possible without losing adequate spatial resolution, and corresponds to a large scale Reynolds number Re $\sim$ 2000. The effective experimental Reynolds number may be higher (e.g., [17]) but is difficult to quantify due to limited spatial resolution as well as the complexity of kinetic effects.

The digitized charge distribution from the CCD camera is normalized to the initial average charge density, yielding a dimensionless vorticity field with $C = 1$ at $t = 0$. (These units are employed throughout the Letter.) The 2D NS code uses these data as initial conditions. This procedure was carried out for a variety of electron trap results (see e.g., Table I), and the time evolution of the experiment was compared with the simulation using the above normalization and correspondence of charge and vorticity. Most of the results shown here are from run BZ, which is typical of all experimental runs except those with very low levels of turbulence. As seen in Fig. 1, the behavior of global quantities in the simulation is very close to the experiment. In the simulations, the computed variation of the ideal invariants C, E, and L is $<1.5\%$. Figure 2 compares the experimental charge density pattern and the vorticity in the simulation at several times. The spatial distribution of charge density progresses through mergers towards a simpler, nearly-axisymmetric state; the vorticity mergers follow this pattern as well. This correspondence (see Fig. 1) lends further empirical evidence that the two systems, NS and MPT, have very similar dynamical relaxation properties, and that Eq. (2) is a relevant dynamical description.

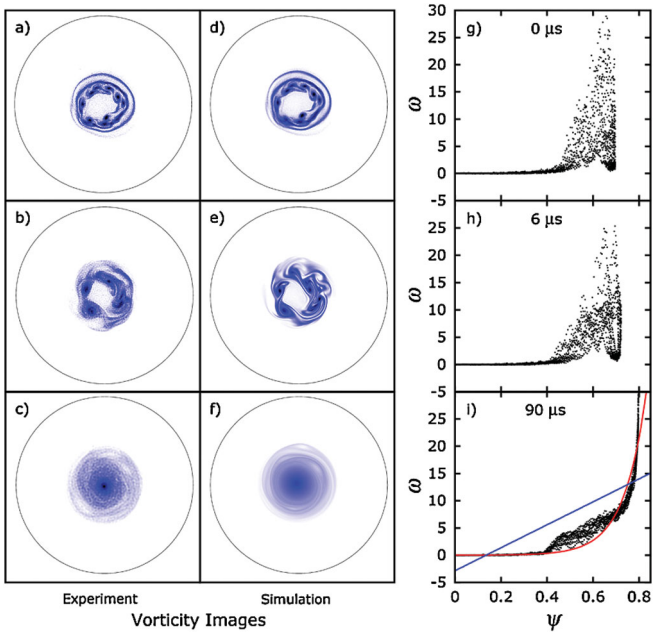

FIG. 2 (color). State of experimental run BZ at three times, $t = 0$, 15, and 90 (μs). Left column: charge density from experiment; Middle column: vorticity from hydrodynamic simulation at the same (inferred) times as the left column; Right column: scatter plots of ω vs ψ, with linear (blue) and exponential (red) fits; see text.

Having established this connection, we seek to further explain the relaxation process seen in Fig. 2.

Previously it was demonstrated [18] that the relaxed states of the periodic (two-signed vorticity) NS equation are given by a functional relationship between ω and ψ that corresponds to a maximum entropy principle. Here (see Fig. 2) scatter plots of ω vs ψ also show a characteristic evolution from a spread distribution towards a single-valued distribution. This suggests an approach to a nonlinear, steady or force-free condition (neglecting dissipation) signified by the single-valued relationship $\omega = \omega(\psi)$. The collapse to a near single-valued $\omega(\psi)$ is reflected in the sequence of vorticity or charge images in Fig. 2. At early times the quasi-isolated vortices are connected by filaments leading to a broad spread of the ω vs ψ distribution. As time progresses, the sequence of vortex mergers and filament interactions causes a narrowing of the ω vs ψ distribution. The single-valued distribution is associated with emergence of a single, strong, nearly axisymmetric vortex. The NS simulations also collapse to a near single-valued $\omega(\psi)$ (not shown). Note that the final form of $\omega(\psi)$ appears to be more an exponential type, rather than linear, apparently favoring the Max-S prediction (cf. [16]).

To understand this relaxation process in greater detail, and to quantitatively distinguish between Max-S and Min-Ω formulations, we proceed to further analysis. A direct approach would be to solve exactly the Min-Ω and Max-S problems, and then compare the solutions to the experimental final state [Fig. 2(i)]. Solutions of Eq. (3) are given by linear combinations of Bessel functions, once C, E, and L are specified. This complete solution [25] does not preserve single-signed charge (vorticity), leading to a proposed solution [2] and its criticisms [16] alluded to above—a fully correct solution would enforce one-signed charge at the onset. On the other hand, Eq. (4) has also not been solved analytically. Even numerically this equation is difficult due to the presence of bifurcations [29]. One special case avoids these problems, namely the axisymmetric solution, Eq. (5).

Since neither theory is amenable to an analytical treatment, we compute least squares fits of the experimental data to the functional forms of the theoretical models. Goodness of fit is assessed graphically and in terms of two- and three-parameter statistics, where parameters are associated with C, E, and if included, L. To evaluate the Max-S and the Min-Ω formulations we optimize the fit parameters in Eqs. (3) and (4) constraining C, E, and L to agree with experiment [30]. Thus, starting from the experiment itself, we can directly estimate α, β and γ in Eq. (4), and δ, ξ and η for Eq. (3).

Figure 3 presents best Max-S and Min-Ω theoretical fits for experimental data set BZ, as well as the experimental profile $\omega(r)$. Similar analyses were performed on other experimental data, e.g., those in Table I, with similar conclusions. Only constrained fits are shown, but both constrained and unconstrained fits gave comparable re-

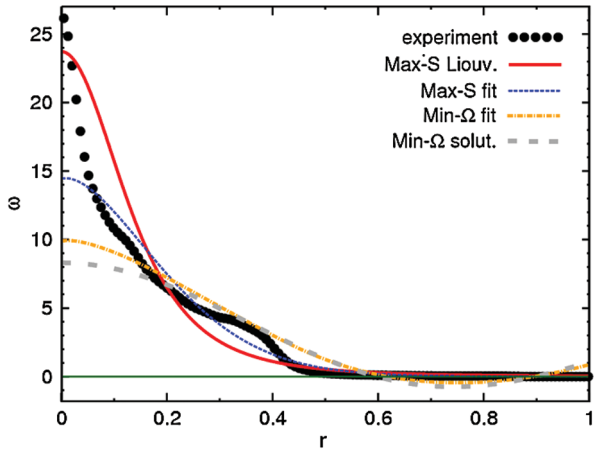

FIG. 3 (color). $\omega(r)$ in experiment BZ (circles) & several theories. Min-Ω fit (thick orange dash), Min-Ω solution (thick gray dash), Max-S Liouville (solid red), Max-S fit (thin blue dash).

sults. See Table I for the normalized squared error of these fits. Figure 3 also shows two exact theoretical predictions for the BZ globals—the exact Min-Ω and Liouville solutions. Both the constrained Max-S fit and the Liouville solution Eq. (5) account well for the experiment.

For every experiment we have analyzed in which the level of turbulence is substantial, the Min-Ω fit is visibly less good than the Max-S fit. In addition the Min-Ω case experiences a physically unallowed change in charge sign, a problem still not satisfactorily resolved. As in the hydrodynamic case [18–20], it has been established that the present data also appear to support the near-maximum entropy principle. In addition to Run D (see Table) we found other cases (not shown) in which a minimum Ω interpretation works reasonably well (cf. [2]); these are cases at lower E/L, which are smoother, have lower Ω, and therefore weaker nonlinear interactions.

The present analysis suggests that for the turbulent systems considered here, relaxation is better described by a maximum entropy principle than by a minimum enstrophy principle. The maximum entropy perspective requires that no *ad hoc* allowances need to be made for the appearance of negative electron densities. The disparity between the two predictions grows as does the intensity of turbulence involved in the relaxation process. This suggests a larger influence of statistical mechanical considerations when the system is free to explore its phase space to a greater extent, as it is in the presence of turbulence. The same idea may explain the differences in our conclusions and those in Ref. [2]; in this regard we plan an analysis of a much larger sample of initial data. We intend to treat this question further in a more comprehensive publication, in which we will also attempt an examination of special metastable states including off axis [15] and isolated vortex [12,14] cases.

This work was supported partially by DOE Grant No. DE-FG02-06ER54853, NASA Space Grant No. NNG05GO92H, and (T. B. M.) by NSF Grant No. PHY-0140318.

*Present address: 103 Cornell Avenue, Swarthmore, Pennsylvania 19081, USA.

[1] C. F. Driscoll and K. S. Fine, Phys. Fluids B **2**, 1359 (1990).
[2] X. P. Huang and C. F. Driscoll, Phys. Rev. Lett. **72**, 2187 (1994).
[3] N. Mattor *et al.*, Phys. Rev. Lett. **96**, 045003 (2006).
[4] G. Joyce and D. Montgomery, J. Plasma Phys. **10**, 107 (1973); D. Montgomery and G. Joyce, Phys. Fluids **17**, 1139 (1974); Y. B. Pointin and T. S. Lundgren, Phys. Fluids **19**, 1459 (1976).
[5] S. Edwards and J. Taylor, Proc. R. Soc. A **336**, 257 (1974).
[6] J. B. Taylor, Phys. Rev. Lett. **33**, 1139 (1974).
[7] W. H. Matthaeus and D. Montgomery, Ann. N.Y. Acad. Sci. **357**, 203 (1980).
[8] R. H. Kraichnan and D. Montgomery, Rep. Prog. Phys. **43**, 547 (1980).
[9] J. Heyvaerts and E. R. Priest, Astron. Astrophys. **137**, 63 (1984).
[10] J. C. McWilliams *et al.*, Science **264**, 410 (1994).
[11] Z. Yin *et al.*, Phys. Fluids **15**, 1937 (2003).
[12] C. F. Driscoll *et al.*, Phys. Scr. **T84**, 76 (2000).
[13] D. Z. Jin and D. H. E. Dubin, Phys. Rev. Lett. **84**, 1443 (2000).
[14] Y. Kiwamoto *et al.*, Phys. Rev. Lett. **99**, 115002 (2007).
[15] E. Sarid *et al.*, Phys. Rev. Lett. **93**, 215002 (2004).
[16] H. Brands *et al.*, Phys. Fluids **11**, 3465 (1999); P. H. Chavanis and J. Sommeria, J. Fluid Mech. **314**, 267 (1996).
[17] Y. Kawai *et al.*, Phys. Rev. E **75**, 066404 (2007).
[18] D. Montgomery *et al.*, Phys. Fluids A **4**, 3 (1992).
[19] W. H. Matthaeus *et al.*, Physica (Amsterdam) **51D**, 531 (1991).
[20] D. Montgomery *et al.*, Phys. Fluids A **5**, 2207 (1993).
[21] J. M. Kriesel and C. F. Driscoll, Phys. Rev. Lett. **87**, 135003 (2001).
[22] C. F. Driscoll *et al.*, Phys. Rev. Lett. **60**, 1290 (1988).
[23] R. A. Smith and T. M. O'Neil, Phys. Fluids B **2**, 2961 (1990).
[24] R. A. Smith, Phys. Rev. A **43**, 1126 (1991).
[25] B. M. Boghosian, Phys. Rev. E **53**, 4754 (1996).
[26] T. S. Levi and D. C. Montgomery, Phys. Rev. E **63**, 056311 (2001).
[27] S. Servidio *et al.*, Phys. Plasmas **15**, 012301 (2008).
[28] S. Li *et al.*, Theor. Comput. Fluid Dyn. **9**, 167 (1997).
[29] B. Marder and H. Weitzner, Plasma Phys. **12**, 435 (1970).
[30] We use a steepest descent method, W. H. Press *et al.*, *Numerical Recipes* (Cambridge U. Press, New York, 1986).